Laserinduced fluorescence study of the reactions Cu+X2→CuX+X (X=F, Cl, Br, and I)

C. C. Fang and J. M. Parson

Citation: The Journal of Chemical Physics **95**, 6413 (1991); doi: 10.1063/1.461561
View online: http://dx.doi.org/10.1063/1.461561
View Table of Contents: http://scitation.aip.org/content/aip/journal/jcp/95/9?ver=pdfcov
Published by the AIP Publishing

Laser-induced fluorescence study of the reactions $Cu + X_2 \rightarrow CuX + X$ ($X = F$, Cl, Br, and I)

C. C. Fang[a] and J. M. Parson
Department of Chemistry, Ohio State University, Columbus, Ohio 43210

(Received 14 June 1991; accepted 19 July 1991)

Reactions of a beam of Cu with halogen gases at low pressure have been studied in the single-collision regime using a pulsed tunable dye laser to excite the ground electronic state products to fluorescing states. CuF vibrational state populations could be estimated up to $v = 25$, but for the heavier halides information on only $v \leqslant 3$ was obtainable from the excitation spectra. The vibrational distributions are similar to prior expectations but somewhat colder. Spectral simulations also reveal that the fraction of energy available to products appearing as rotation is considerably below prior predictions. This pattern of energy release may be related to product repulsion, which occurs as the products transform from a strongly bound XCuX intermediate to the singly ionic ground state molecule plus halogen atom.

I. INTRODUCTION

Gas phase reactions of copper with halogen gases have been studied since the early 1970's. Most of the kinetics work has involved the observation of visible chemiluminescence (CL), that is, probing the nascent upper electronic state products. Experiments have ranged from the high pressure multicollision environments of shock tubes[1] and flow systems[2] to the low pressure single-collision regime of molecular beams.[3,4]

Schwenz and Parson[3] reported the first molecular beam studies of energy disposal in reactions of ground state Cu with F_2. Partitioning of product energy into electronic, vibrational, and rotational energies was determined. Baltayan, *et al.*[5,6] observed more efficient CL in reaction of metastable Cu (^2D) formed in a flow system by sputtering inside a hollow cathode discharge. The presence of emission from high-lying vibrational states allowed the extraction of improved vibrational and rotational constants for CuF. Optical pumping of the metastable Cu states subsequently allowed assignment of particular states ($^2D_{3/2}$ or $^2D_{5/2}$) as sources of the emitting products.[6] Parson and Fang[7] observed the same reactions under molecular beam conditions utilizing a dc discharge at the oven orifice as a source of metastable Cu. They were able to compare the effects of increasing electronic and translational energy on product state distributions.

Flow experiments using a Broida-type metal source were used to follow CL of CuCl and CuBr.[8,9] Photon yields, however, were very low, and no reaction mechanisms were proposed for the endothermic processes necessary to give CL. Beam-gas studies of the CL reactions with Cl_2, Br_2, and I_2 utilizing time-of-flight (TOF) measurements and variations in copper source temperature addressed the question of what the reactive copper species might be.[4] Present in a thermal beam were dimers and metastable atoms, and the CL could be attributed entirely to the metastable atoms. CL from the *A*, *B*, *C*, *D*, and *E* states of CuCl, the *A* and *B* states of CuBr, and *A*, *C*, and *D* states of CuI was reported. Subsequent experiments utilized the same discharge source for metastable Cu as in the $Cu + F_2$ study.[10] Some computer simulations of the spectra, in which numerous sequences are extensively overlapped, have been performed in an attempt to determine product vibrational energy distributions.

Laser-induced fluorescence (LIF) signals of CuX ($X = Cl$, Br, and I) from the $Cu + X_2$ reactions were obtained earlier in this laboratory by using a cw dye laser with a bandwidth of about 1 Å.[11] Computer simulations were made of the CuCl spectra. The amount of energy appearing as rotation and vibration of CuX was found to be unusually small. Higher resolution spectra were needed for better characterization of the rotational energy distributions. The background caused by CL was too intense in the $Cu + F_2$ reaction to allow cw detection of CuF by LIF. Consequently, we have chosen to use a pulsed dye laser for further LIF studies so that most of the CL could be removed by gated detection. In contrast to the CL reactions, the ground state reactants correlate adiabatically to the ground state products detected in this LIF study.

Table I gives spectroscopic constants for the electronic states used in the current LIF study, and radiative lifetimes of the upper levels. There has been considerable controversy on the electronic assignments, particularly for the lowest excited electronic states, which are not used in this study, but *ab initio* theoretical results and experimental radiative lifetimes have been used recently to confirm or modify earlier assignments of electronic states based on rotational structure.[12–17] State designations given in Table I are now generally accepted, although mixing with other electronic states is extensive and the source of much of the original uncertainty.

II. EXPERIMENTAL ARRANGEMENT

Figure 1 shows a schematic diagram of the experimental configuration. The major components are a molecular beam system, an excimer-pumped tunable dye laser, a gated pho-

[a] Present address: QO Chemicals, Inc., P.O. Box 759, Belle Glade, Florida 33430.

TABLE I. Spectroscopic constants in cm^{-1} for CuX and excited state radiative lifetimes (τ, μs).

Molecule	Constant	Electronic state		
CuF		$X(^1\Sigma^+)^{a,b}$	$C(^1\Pi)^{b,c,d}$	
	T_e	···	20 258.1	
	ω_e	620.87	643.83	
	$\omega_e x_e$	3.365	3.715	
	$\omega_e y_e$	0	0.0149	
	$\omega_e z_e$	0.000 28	−0.000 46	
	B_e	0.379 408	0.374 77	
	$10^3\alpha_e$	3.2297	2.8766	
	$10^5\gamma_e$	1.230	−0.69	
	$10^7 D_e$	5.655	5.33	
	$10^9\beta_e$	1.2	1.2	
	τ	···	0.6	
CuCl		$X(^1\Sigma^+)^a$	$D(^1\Pi)^{a,d}$	$E(^1\Sigma^+)^{a,d}$
	T_e	···	22 969.74	23 074.24
	ω_e	415.29	392.89	403.30
	$\omega_e x_e$	1.580	1.745	1.620
	$\omega_e y_e$	0	0	−0.0093
	B_e	0.1763	0.1678	0.1663
	$10^3\alpha_e$	1.0	0.98	1.08
	$10^6\gamma_e$	2.0	0	0
	τ	···	0.45	0.43
CuBr		$X(^1\Sigma^+)^a$	$B(^1\Pi)^{a,e}$	$C(^1\Sigma^+)^{a,e}$
	T_e	···	23 044.7	23 460.9
	ω_e	314.80	284.22	294.70
	$\omega_e x_e$	0.96	1.32	1.06
	B_e	0.101 93	0.0903	0.0942
	$10^4\alpha_e$	4.5214	4.9	4.1
	$10^7\gamma_e$	7.0	0	0
	τ	···	0.45	0.23
CuI		$X(O^+)^a$	$C(0)^{a,e,f}$	$D(1)^{a,e}$
	Te	···	21 867.3	22 957.5
	ω_e	264.5	229.7	212.8
	$\omega_e x_e$	0.60	0.53	0.930
	B_e	0.0733	0.0682	0.068 77[g]
	$10^4\alpha_e$	2.8	2.2	0
	$10^7\gamma_e$	3.0	0	0
	τ	···	1.0	0.5

[a] Huber and Herzberg (Ref. 12).
[b] Baltayan *et al.* (Ref. 5).
[c] F. Ahmed, R. F. Barrow, A. H. Chojnicki, C. Dufour, and J. Schamps, J. Phys. B **15**, 3801 (1982).
[d] Delaval *et al.* (Ref. 13).
[e] Lefebvre *et al.* (Ref. 15).
[f] K. P. R. Nair, Chem. Phys. Lett. **92**, 271 (1982).
[g] Adjusted for optimal simulation.

ton counting detection system, and an on-line computer. The molecular beam apparatus has been described previously.[3,4,7] An effusive beam of Cu was generated from a cylindrical graphite oven with a graphite crucible that was heated by surrounding it with a tungsten mesh radiator. Throughout these experiments the oven was heated to about 1890 K, as measured by a calibrated optical pyrometer. At this temperature the vapor pressure of Cu in the oven was 0.9 Torr. The beam was collimated by a 6×3 mm slit at 2 cm from the oven orifice, and after an additional 16.5 cm entered the chamber, which contained the halogen reactant.

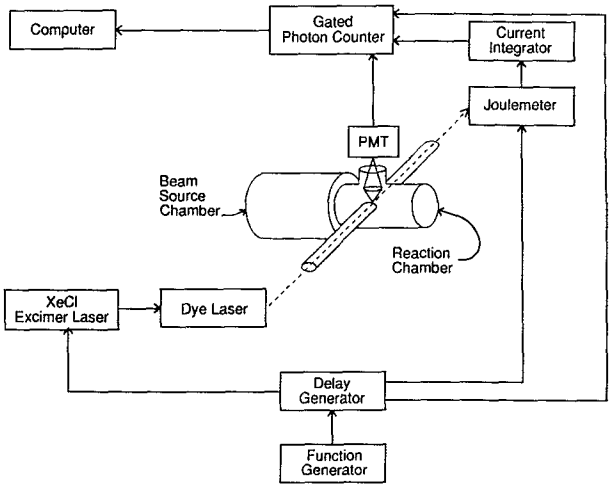

FIG. 1. Schematic diagram of the experimental configuration.

Fluorine from a 50% F_2/He mixture and chlorine were leaked into the reaction chamber with a regulator and a needle valve. Bromine and iodine were obtained from a temperature-regulated flask maintained at 300 and 340 K, respectively. Bromine was leaked through a needle valve into the chamber, while iodine was controlled by adjusting a stopcock at the flask. Heating tape was used around the glass and stainless steel lines connecting the flask to the chamber to prevent condensation. The total pressure in the reaction chamber was typically 10^{-3} Torr, as measured by a capacitance manometer. The gases were trapped between the diffusion pump and the mechanical pump. Fluorine was reacted with heated soda lime, and the other gases were condensed on a liquid nitrogen cooled trap.

The laser system consisted of a tunable dye laser (Lumonics Hyperdye-300) pumped at 125 Hz by 60 mJ pulses from a XeCl excimer laser (Lumonics Excimer-520). Typical dye laser pulse width is about 8 ns, and the maximum bandwidth is less than 0.1 cm^{-1}. The following dye solutions were used: coumarin 420 for CuCl and CuBr, coumarin 440 and coumarin 460 for CuI, and coumarin 480 for CuF. The upper electronic states excited by the laser all have short radiative lifetimes, as seen in Table I.

The pulse timing was controlled by a square wave generator that triggered the excimer laser, a pyroelectric joulemeter for monitoring the dye laser power (Molectron J25HR), and a photon counter (Stanford Research SR-400), which was gated for measuring the fluorescence during an adjustable time period.

The dye laser beam was collimated and weakly focused. It entered and exited the reaction chamber through Brewster's angle quartz flats on side arms containing blackened baffles to minimize scattered light. A set of neutral density filters was used to avoid saturation of the transitions or of the photon counting detection system. The filter density was increased until the induced fluorescence was proportional to

the laser power. The laser beam intersected the Cu beam at 90°, and the power was monitored after the exit side arm. The induced fluorescence was focused through a lens onto a water-cooled photomultiplier tube (PMT) (EMI 9789QB), oriented perpendicular to the laser beam and the Cu beam.

The amplified pulses from the PMT were sent to channel A of the gated photon counter. The counting gate was opened for three times the radiative lifetime of the copper halides immediately after the scattered laser light signal diminished. In a fast scan mode each data point was collected for over 1000 successive laser pulses, while the laser was scanned through about 0.2 Å. In a slow scan mode used to resolve rotational structure, the laser scanned through about 0.022 Å during each counting period. The laser power signal was converted to a digital pulse train, which was counted by channel B during the same time intervals that the fluorescence signal was accumulated in channel A.

A 520 nm cutoff interference filter, placed between the focusing lens and the PMT, was used to minimize background signal due to scattered laser light, oven light, and CL from the reactions of Cu with F_2, and $Cu^*(^2D)$ with Cl_2, Br_2, and I_2. The LIF signal was transferred to an IBM XT compatible computer. The computer was used to subtract the background signal, to correct for variations of laser power during data acquisition, and to store the spectra for further analysis. Periodic interruption of the LIF scans were made to measure the background signal and variations in the signal due to drifts in the copper and halogen number densities.

III. EXCITATION SPECTRA

The observed LIF spectra of the copper halide reaction products are shown in Figs. 2–8. These spectra have been corrected for variations in laser power and in copper and halogen densities. All the spectra can be assigned to previously characterized electronic transitions.

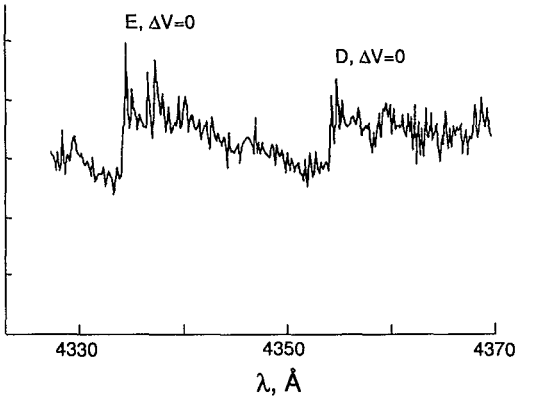

FIG. 3. Experimental excitation spectrum of the CuCl D–X and E–X transitions.

Figure 2 shows the $\Delta v = 0$ sequence C–X transition of CuF, as well as a small contribution of the B–X transition. Vibrational levels are substantially populated from low-lying states all the way to at least the state that gives a head of heads within a sequence ($v = 22$ in the $\Delta v = 0$ sequence at 4854 Å). The level populations differ significantly from those observed in CL from reaction of either the ^2S or ^2D states of Cu. At low vibrational levels, the Q heads are the most prominent features, and the R heads appear as the head of heads is approached.

The $\Delta v = 0$ sequences of the D–X and E–X electronic transitions of CuCl product are shown in Fig. 3. The $Cu + Cl_2$ reaction has been studied using different Cl_2 pressures. The spectrum in Fig. 3 was taken at 1 mTorr. For pressures above 2 mTorr, the bandheads tend to sharpen, indicating relaxation of the rotational state distribution. The higher pressure scans appear similar to spectra obtained by Rosano earlier in this laboratory using a cw dye laser.[11]

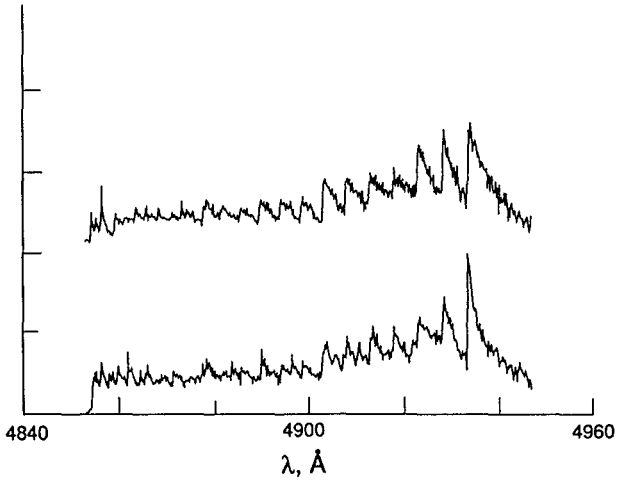

FIG. 2. Excitation spectrum of the CuF C–X transition, $\Delta v = 0$ sequence. Relative photon count is plotted versus excitation wavelength. The lower panel is experimental, and the upper is computer simulated.

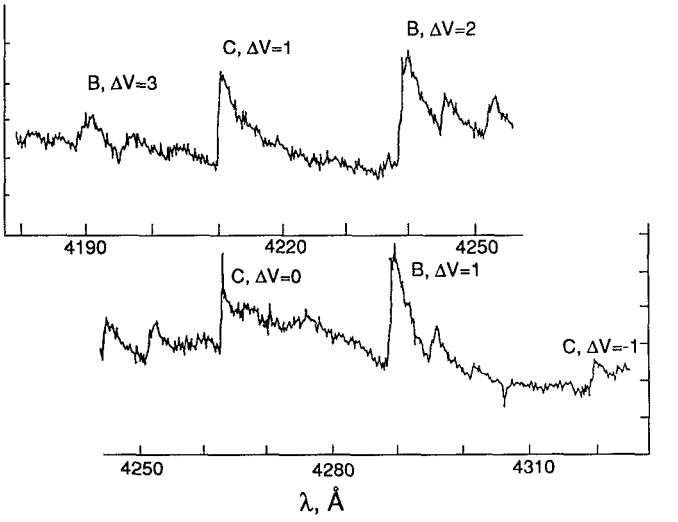

FIG. 4. Experimental excitation spectrum of the CuBr B–X and C–X transitions.

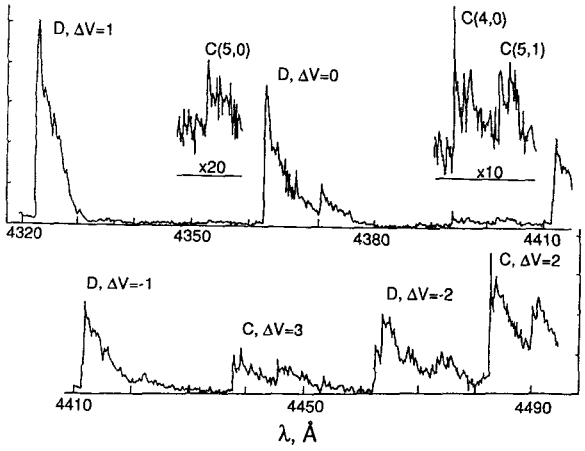

FIG. 5. Experimental excitation spectrum of the CuI C–X and D–X transitions with coumarin 440 dye solution.

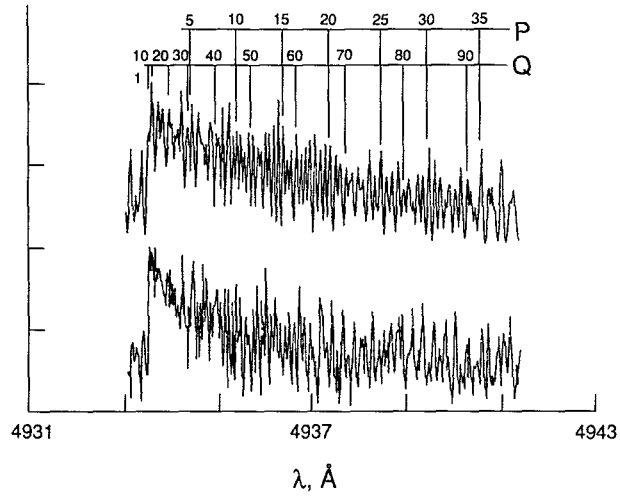

FIG. 7. Excitation spectrum of the CuF C–X (0,0) band with rotational resolution. The lower panel is experimental, and the upper is computer simulated.

There is still considerable unstructured underlying LIF even after correcting for the PMT dark count, oven light, and CL signal. This may be due to other sequences since there is sufficient energy available to populate vibrational levels up to $v = 30$, and off-diagonal Franck–Condon factors become more significant at higher vibrational levels.

The CuBr product spectrum is shown in Fig. 4. The $\Delta v = +1$, $+2$, and $+3$ sequences of the B–X electronic transition, and the $\Delta v = -1$, 0, and $+1$ sequences of the C–X transition are assigned in the figure. This spectrum, like the CuCl one, also displays an underlying background.

The CuI product was detected by excitation of the C–X and D–X systems that lie between 432 and 465 nm. Figure 5 shows the scan obtained with coumarin 440 dye. The $\Delta v = +2$ to $+5$ sequences of the C–X transition and the $\Delta v = -2$ to $+1$ sequences of the D–X transition are evident. The $\Delta v = -1$ to $+2$ sequences of the C–X transition and the D–$X(0,3)$ band are shown in the spectrum in Fig. 6, which was obtained by scanning with coumarin 460 dye.

IV. COMPUTER SIMULATIONS

The LIF technique is an attractive method for detecting molecular species and determining their internal state distributions. The procedure for extracting relative populations from the variation of the LIF signal with laser wavelength (laser excitation spectrum) has been described extensively.[18–20] In our experiments essentially all of the laser excited molecules radiated in the time allowed for detection, and the PMT response was nearly constant over the wavelength range for most of the emission. In this case the relative LIF signal simplifies to

$$I(\nu) \propto N(v''J'')\rho_\nu q_{v'v''}\,[S_{J'J''}/(2J''+1)],$$

where $N(v''J'')$ is the X state population, ρ_ν is the laser energy at the excitation frequency ν from state $v''J''$ to state $v'J'$,

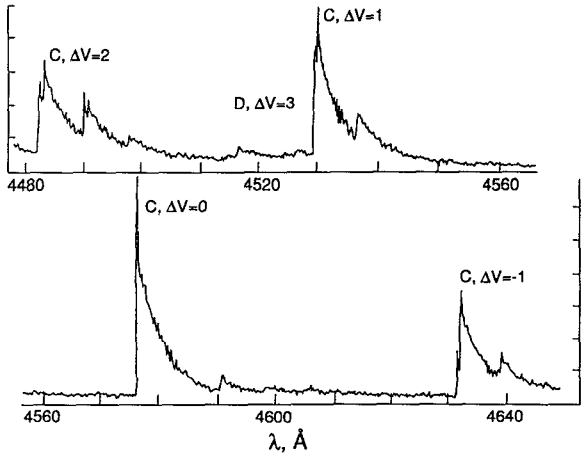

FIG. 6. Experimental excitation spectrum of the CuI C–X transition with coumarin 460 dye solution.

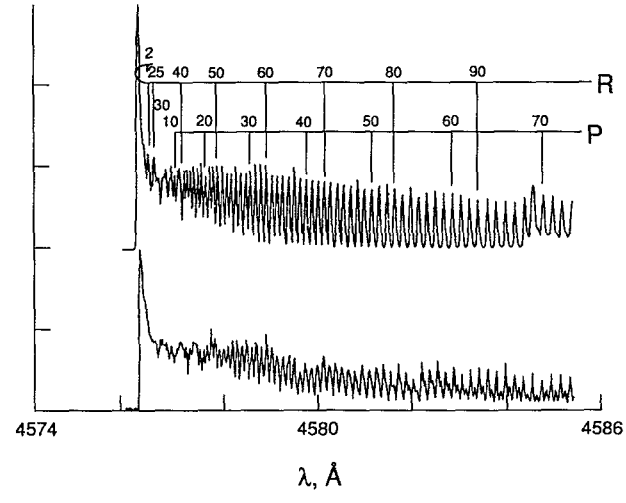

FIG. 8. Excitation spectrum of the CuI C–X (0,0) band with rotational resolution. The lower panel is experimental, and the upper is computer simulated.

$q_{v'v''}$ is the Franck–Condon factor (FCF), and $S_{J'J''}$ is the Hönl–London factor. More complicated treatments would be necessary if partial saturation of the transitions had occurred or if there were major differences in the radiative lifetimes of the states excited. A computer program was needed to extract information on the populations from the LIF signal because of extensive overlap of the rotational lines. All the necessary FCF's of the copper halides were calculated using Rydberg–Klein–Rees potentials, which were generated from available spectroscopic constants. In some cases FCF's were required for levels that are above those used in the determination of the constants, and this increased uncertainties in the FCF's. Also, FCF's for only rotationless vibrational states were used. The rotational line strengths were calculated using standard expressions.[21] A Boltzmann thermal distribution was used for the rotational distributions, truncated for each vibrational state at the maximum rotational quantum number dictated by the energy available. The rotational temperature and individual vibrational state populations were varied by a nonlinear least-squares fitting procedure.[22] The spectroscopic constants used are listed in Table I.

The simulation result for the CuF excitation spectrum is shown in Fig. 2. Only the $\Delta v = 0$ sequence of the C–X transition was chosen for simulation since the FCF's are close to unity and are better known for this sequence, and the better signal to noise makes the experiment more reliable. The rotational temperature obtained from the simulation is 3387 K. Overlapping of vibrational bands was too extensive to allow investigation of whether the temperature should be allowed to vary with vibrational state. The experimental spectrum in the (0,0) band is seen to be sharper than the calculated one. This may be due to some collisional relaxation of the rotational distribution prior to laser excitation. The positions of the calculated bandheads of all the vibrational states are well matched with those of the experimental spectrum. However, there is some disagreement between the band shapes of the experimental spectrum and the computer simulated spectrum at high vibrational states. This may be a result of (i) some contribution from the B–X transition in the shorter wavelength region, (ii) inaccuracies in the rotational constants for higher vibrational levels, and (iii) inability of the Boltzmann distribution to represent the rotational state populations.

For the heavier copper halides, simulations were performed using more than one sequence and electronic transition. The computer simulated spectra are given elsewhere.[23] Table II lists all of the sequences simulated and rotational temperatures of the ground electronic state products based on each simulation. Although uncertainties in the rotational temperatures are difficult to quantify, agreement of the rotational temperatures obtained using different sequences is reasonable in light of the experimental noise and the varying contribution of different vibrational states. The large discrepancy between the temperature found for the C–X $\Delta v = 0$ sequence of CuBr and the other CuBr results is most likely caused by interference in this sequence from the $\Delta v = 2$ sequence of the B–X transition, making the background correction procedure unreliable.

TABLE II. Sequences simulated and rotational temperatures.

Molecule	Transition	Sequence	T_{rot} (K)
CuF	C–X	0,0	3387
CuCl	D–X	0,0	1547
	E–X	0,0	1606
CuBr	B–X	1,0	197
	B–X	2,0	276
	C–X	0,0	830
	C–X	1,0	383
CuI	C–X	0,0	324
	C–X	1,0	316
	C–X	2,0	383
	C–X	3,0	452
	D–X	0,0	490
	D–X	0,1	511

Single bands were simulated for CuF and CuI in cases that had minimal overlap with other bands. Figure 7 compares the experimental spectrum of the CuF C–X(0,0) band with the computer simulated spectrum in the upper panel, and Fig. 8 makes the same comparison for the CuI C–X(0,0) band. The contours in the experimental spectra and the simulated spectra are seen to be similar. The rotational temperature in the CuF simulation was 2357 K, which is less than 3387 K obtained from the simulation of the entire $\Delta v = 0$ sequence. This discrepancy can be attributed to the fact that this single-band simulation extended only to the $P(90)$ transition, whereas the full-sequence fit involved all the energetically accessible rotational levels up to $J = 263$. The rotational temperature in the CuI simulation is 350 K, which is very close to 324 K obtained from simulation of the entire $\Delta v = 0$ sequence observed. The unmatched lines in the experimental spectra in the higher wavelength portions may be due to the Cu isotope splitting or transitions in other bands, which were not included in the simulation.

V. POPULATION ANALYSIS

The LIF signal observed under nonsaturated conditions is proportional to the product number densities instead of the product flux densities. It is product flux density that is proportional to the detailed rate coefficient for forming the product states. In order to obtain the relative rate coefficients for forming the product internal states, conversion of product number density to flux density has to be performed. This requires knowledge of the angular and velocity distributions of the scattered products. Although this information is not available for these reactions, one can achieve an approximate conversion of densities by using a Newton diagram to estimate the product velocity based on two extreme cases of forward and backward scattering of the CuX molecule in the center-of-mass frame. Although a beam-gas configuration has been used, 90° collisions are expected to be representative of the average results when all collision angles are considered. The laboratory velocity of every individual

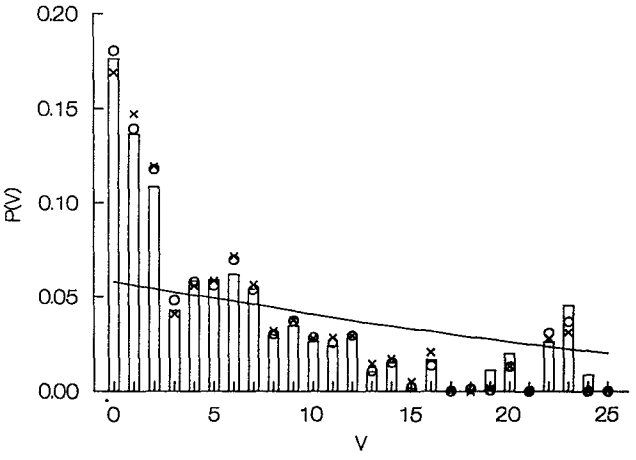

FIG. 9. Vibrational distribution, $P(v)$, for CuF. The vertical bars give the results using a Boltzmann rotational distribution, the crosses the results using the Prior model[24] for the rotational distribution, and the circles the results using the alternative empirical form given in the text for the rotational distribution. Normalization of these and other $P(v)$ distributions includes only the states shown. The vibrational distribution from the prior model is given by the solid curve.

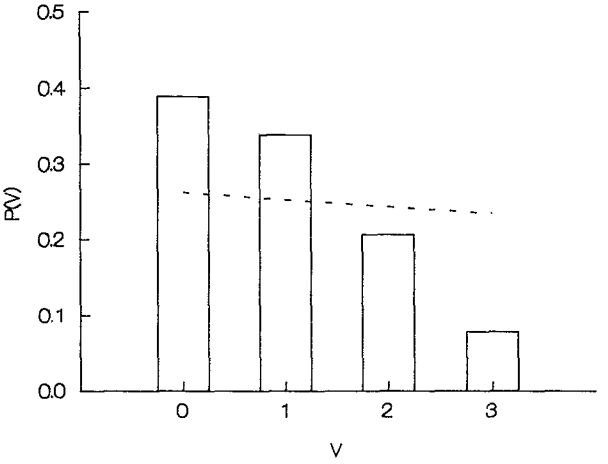

FIG. 11. Vibrational distribution for CuBr. The dashed curve gives the prior prediction.

rotational level is estimated from the Newton diagram assuming forward or backward scattering. The relative number density of each rotational state is multiplied by the estimated laboratory velocity to give a relative flux density. Finally, the integrated result for the flux densities of the complete set of rotational states in this fixed vibrational level gives the relative vibrational flux density. Representative Newton diagrams show that the product velocities are large and similar for the vibrational states that have been probed in these experiments.[23] Hence this correction has only a minor effect on the vibrational distributions, and was judged to be smaller than the uncertainties in the vibrational populations obtained.

Figures 9–12 show the vibrational populations of CuX obtained from the computer simulations. The dashed lines represent distributions based on a prior model. In the rotating-vibrator approximation, the prior expectation for the rotational distribution is given by[24]

$$P_v^0(J) \propto (2J+1)(E_{\text{tot}} - E_{\text{vib}} - E_{\text{rot}})^{1/2},$$

where E_{tot} is the total available energy, E_{vib} is the product vibrational energy, and E_{rot} is the product rotational energy. The prior form for a vibrational state is given by

$$P_v^0 = \sum_J P_v^0(J) \propto B_v^{-1}(E_{\text{tot}} - E_{\text{vib}})^{3/2}.$$

Data presented here are the average results taken from all simulated transitions, with equal weighting of the various results.

Once the CuX internal state distributions are determined, it is straightforward to calculate the average energy

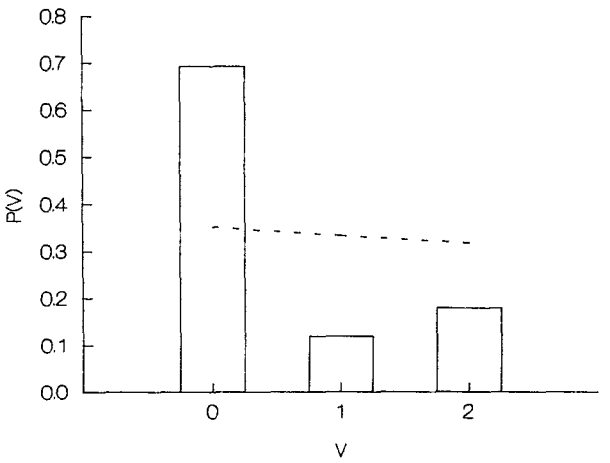

FIG. 10. Vibrational distribution for CuCl. The dashed curve gives the prior prediction.

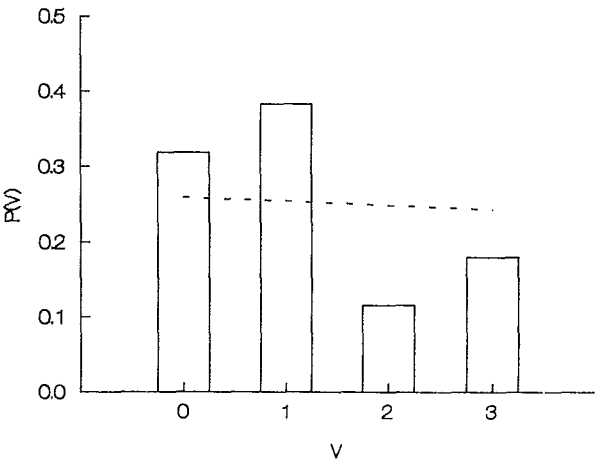

FIG. 12. Vibrational distribution for CuI. The dashed curve gives the prior prediction.

disposed into different degrees of freedom. Since the Boltzmann distribution is used for the rotational degrees of freedom, the average rotational energy for vibrational state v is readily found to be

$$\langle E_{\rm rot}\rangle_v = kT_{\rm rot} - E_{{\rm max},v}/(e^{E_{{\rm max},v}/kT_{\rm rot}} - 1),$$

where $E_{{\rm max},v}$ is the maximum rotational energy available in each vibrational state based on energy conservation. Consequently, the overall average rotational energy is

$$\langle E_{\rm rot}\rangle = \frac{\Sigma_v P(v)\langle E_{\rm rot}\rangle_v}{\Sigma_v P(v)}.$$

The average vibrational energy is calculated using

$$\langle E_{\rm vib}\rangle = \frac{\Sigma_v P(v) E_{\rm vib}(v)}{\Sigma_v P(v)}.$$

It should be noted that all the calculations are done only up to the highest vibrational state observed, even though this value is much less than the highest accessible one. The results are listed in Table III. The fractions of product energy appearing in vibration, rotation, and translation are also included, given as $\langle f_v\rangle$, $\langle f_r\rangle$, and $\langle f_t\rangle$, respectively. The corresponding prior predictions are given with a superscript "0" in the table.

VI. DISCUSSION

A comparison of product energy disposal with the prior model can be used to explore the possibility of unusual dynamical effects in these reactions. We note that the vibrational distributions of CuX obtained in the present study are qualitatively similar to the prior distributions shown in Figs. 10–13. Also, we find general agreement between experiment and prior predictions for the fraction of energy disposed in vibration. A similar extent of agreement has been reported earlier in comparisons of prior predictions with vibrational state distributions found for the A, B, and C states of CuF formed in the CL reaction of Cu(^2S) with F_2.[3] It was suggested that the agreement there might be due to the reactions proceeding by way of the FCuF ground state of the collision complex, which would be expected to live long enough for energy randomization to occur. The results were in sharp contrast to the highly inverted vibrational distributions formed when the ^2D states of Cu react with F_2.

On close inspection one sees that the experimental X state vibrational distributions generally show higher populations at low vibrational levels than the prior model. The correction from number density to flux density, if it could be done accurately, is not expected to improve the agreement since lower v levels are likely to have higher velocities and hence even larger densities after correction.

Since the rotational distributions are only crudely determined in the simulations, two alternative forms for the rotational distribution were chosen to see whether the CuF vibrational distribution depended strongly on the choice of rotational distribution. In Fig. 11 the crosses indicate the CuF vibrational distribution that was determined using the prior form given above for the rotational distribution, and the circles indicate the results found using the form

$$P_v(J) \propto (2J+1)(1 - J/J_{{\rm max},v})^n,$$

with n a variable parameter. All three results for vibrational distribution are seen to be nearly the same.

The rotational temperatures found for CuF and CuCl were quite high, 3387 and 1575 K, respectively. Table III shows, though, that rotational excitation is less than the prior model predicts for both reactions. Considerably colder rotational distributions were found for CuBr (420 K) and CuI (413 K), giving much larger deviations from prior distributions. The rotational distributions for these heavier halides are possibly less accurately known because increased mixing of singlet radiative states with nearby triplet states makes the simple singlet–singlet Hönl–London factors less appropriate.

Clearly, a simple application of the prior model, or more elaborate statistical calculations such as phase-space theory, will not be adequate for explaining all the results presented here. The tendency to form cold rotational distributions may be related to limitations on high J states imposed by the reactivity dependence on impact parameter. If only small impact parameters lead to reaction, then angular momentum conservation may limit the final J value unless the final orbital and rotational angular momentum tend to be oriented in opposite directions. One does not expect these two momenta to oppose each other for separation of a near collinear complex ($C_{\infty v}$ or C_{2v} symmetry). Low rotational and vibrational excitation of the products could also be attributed to a potential energy surface that directs the energy of an exit channel barrier into product translation. If the lowest adiabatic surface is followed throughout, one might expect a barrier in the region where the intermediate must change from the doubly ionic XCuX structure to the singly ionic ground state molecule plus halogen atom.

Although this study presents only a coarse picture of the internal state distributions, it points toward the need for potential energy surfaces and dynamical models in order to characterize these reactions. In comparison with earlier work, the most significant changes in vibrational distributions appear to arise when different atomic states are reacted rather than merely different product electronic states are formed.

TABLE III. Characteristics of product energy distributions for the vibrational states included in the spectral simulations. The last three rows give the prior model results.

	CuF	CuCl	CuBr	CuI
$E_{\rm tot}$, kJ/mol	285	157	163	192
$\langle E_v\rangle$, kJ/mol	46	2.4	3.6	2.5
$\langle E_r\rangle$, kJ/mol	28	13	3.5	3.1
$\langle f_v\rangle$	0.16	0.015	0.022	0.013
$\langle f_r\rangle$	0.098	0.084	0.021	0.016
$\langle f_t\rangle$	0.74	0.90	0.96	0.97
$\langle f_v^0\rangle$	0.245	0.0305	0.0333	0.0241
$\langle f_r^0\rangle$	0.297	0.381	0.382	0.387
$\langle f_t^0\rangle$	0.458	0.588	0.587	0.589

ACKNOWLEDGMENTS

Support of the National Science Foundation is gratefully acknowledged. We would like to recognize the contributions of Dr. William Rosano in measuring and analyzing cw LIF spectra from reactions of Cu with Cl_2, Br_2, and I_2.

[1] S. E. Johnson, P. B. Scott, and G. Watson, J. Chem. Phys. **61**, 2834 (1974).
[2] R. E. Steele and H. P. Broida, J. Chem. Phys. **69**, 2300 (1978).
[3] R. W. Schwenz and J. M. Parson, J. Chem. Phys. **73**, 259 (1980).
[4] R. W. Schwenz and J. M. Parson, Chem. Phys. Lett. **71**, 524 (1980).
[5] P. Baltayan, F. Hartmann, J. C. Pebay-Peyroula, and N. Sadeghi, Chem. Phys. **120**, 123 (1988).
[6] P. Baltayan, F. Hartmann, I. Hikmet, J. C. Pebay-Peyroula, and N. Sadeghi, Chem. Phys. Lett. **160**, 549 (1989).
[7] J. M. Parson and C. C. Fang, J. Chem. Phys. **92**, 4823 (1990).
[8] G. A. Capelle, R. S. Bradford, and H. P. Broida, Chem. Phys. Lett. **21**, 418 (1973).
[9] S. Rosenwaks, Chem. Phys. Lett. **64**, 352 (1979).
[10] E. J. Wall, M. S. thesis, The Ohio State University, 1987.
[11] W. J. Rosano, Ph.D. dissertation, The Ohio State University, 1985.
[12] K. P. Huber and G. Herzberg, *Molecular Spectra and Molecular, IV. Constants of Diatomic Molecules* (Reinhold, New York, 1979).
[13] J. M. Delaval and J. Schamps, Chem. Phys. **111**, 129 (1987).
[14] J. M. Delaval and J. Schamps, Chem. Phys. **100**, 21 (1985).
[15] Y. Lefebvre, J. M. Delaval, P. Bernage, and P. Niay, Chem. Phys. Lett. **139**, 212 (1987).
[16] A. Ramírez-Solis, J. P. Daudey, and C. Teichteil, J. Chem. Phys. **93**, 7277 (1990).
[17] A. Ramírez-Solis and J. P. Daudey, Chem. Phys. **134**, 111 (1989).
[18] K. Liu and J. M. Parson, J. Chem. Phys. **67**, 1814 (1977).
[19] R. N. Zare and P. J. Dagdigian, Science **185**, 739 (1974).
[20] R. Altkorn and R. N. Zare, Annu. Rev. Phys. Chem. **35**, 265 (1984).
[21] I. Kovacs, *Rotational Structure in the Spectra of Diatomic Molecules* (Elsevier, New York, 1969).
[22] F. James and M. Roos, Comput. Phys. Commun. **10**, 343 (1975).
[23] C. C. Fang, Ph.D. dissertation, The Ohio State University, 1989.
[24] R. B. Bernstein and R. D. Levine, Adv. At. Mol. Phys. **11**, 216 (1975).